

Thermoelectric properties of n -type SrTiO_3

Jifeng Sun and David J. Singh*

Department of Physics and Astronomy, University of Missouri, Columbia, Missouri 65211-7010, USA

(Dated: November 13, 2021)

We present an investigation of the thermoelectric properties of cubic perovskite SrTiO_3 . The results are derived from a combination of calculated transport functions obtained from Boltzmann transport theory in the constant scattering time approximation based on the electronic structure and existing experimental data for La-doped SrTiO_3 . The figure of merit ZT is modeled with respect to carrier concentration and temperature. The model predicts a relatively high ZT at optimized doping, and suggests that the ZT value can reach 0.7 at $T = 1400$ K. Thus ZT can be improved from the current experimental values by carrier concentration optimization.

PACS numbers:

I. INTRODUCTION

Thermoelectric (TE) energy conversion has been widely recognized as a promising technology in power generation including waste heat recovery^{1–3}. However the applications are limited due to the low efficiency. This is associated with the dimensionless figure of merit $ZT = \sigma S^2 T / \kappa$, where σ is the electrical conductivity, S is the Seebeck coefficient, T is the temperature and κ is the thermal conductivity. Oxides may offer advantages in applications.^{4–7} However, while there are a number of thermoelectric materials with $ZT > 1$ ^{8–10}, progress in oxide thermoelectrics has been slower.

Oxide thermoelectrics with high ZT value approaching 1 mainly fall in p -type Co oxides and related alloys^{11–14}. n -type oxide thermoelectrics with high performance are rare and with ZT value barely exceeding 0.5. The best n -type to date is found in ZnO ceramics at high temperatures^{15–18}. Among the several n -type oxides, SrTiO_3 (STO) with cubic perovskite structure has attracted growing attention for TE power generation at high temperatures due to its large Seebeck coefficient originated from the degenerate Ti $3d$ - t_{2g} band at the conduction band minimum and high power factor (PF) comparable to that of Bi-Te alloy¹⁹. However the ZT value achieved is still quite low (< 0.5) even at 1000 K. This is mainly attributed to its high thermal conductivity ($6\text{--}12 \text{ Wm}^{-1}\text{K}^{-1}$ for undoped STO²⁰). Optimizing the doping level and elements as well as introducing point defects are effective methods to reduce the thermal conductivity. For instance the La- and Nb-doped STO can have κ as low as $3 \text{ Wm}^{-1}\text{K}^{-1}$ at about 1000 K depending on the doping concentrations²¹. Lower thermal conductivity down to $2.3 \text{ Wm}^{-1}\text{K}^{-1}$ at 1073 K can be achieved through double doping with La and Dy on the Sr (A) site²². The ZT at corresponding temperature is reported to be 0.36 which is a relatively high value in doped STO. A-site vacancies also can lower κ . Particularly, Popuri *et al.* has shown a glass-like thermal conductivity through A-site vacancies and $\kappa = 2.5 \text{ Wm}^{-1}\text{K}^{-1}$ can be realized at 1000 K²³. Recently, Lu and co-workers find high ZT about 0.4 at 973 K with similar low $\kappa = 2.5 \text{ Wm}^{-1}\text{K}^{-1}$ from their La-doped and A-site-deficient samples²⁴. Importantly, STO has been identified as a material with a corrugated band structure of a form that is particularly beneficial for the electronic part of ZT , but which at the same time is not reasonably described by standard parabolic band models. This makes detailed calculations particularly important.

Here we report on the thermoelectric properties of cubic STO from a combination of first-principles calculations and analysis of existing experimental data. High temperature up to 1400 K was investigated because the thermoelectric performance typically increases with temperature for wide band gap materials. Furthermore, the melting point of STO is high (2080 °C) and n -type STO is expected to be applicable at high temperatures. We find that the optimized n -type ZT can reach a peak value of ~ 0.7 at 1400 K with reasonable high doping concentrations.

II. COMPUTATIONAL METHODS

The model for n -type STO was constructed along the lines of the prior model for PbSe ²⁵. Specifically, the transport functions and coefficients are obtained using a relaxation time approximation to Boltzmann transport theory²⁶ based on first-principles electronic structure. We use the constant scattering time approximation (CSTA) also known as the constant relaxation time approximation, as implemented in the BoltzTraP code²⁷. The CSTA consists in taking the energy dependence of the band structure as the main ingredient in the energy dependence of the conductivity in the transport formula.^{27,28} With this approximation the scattering time cancels in the expression for the thermopower, so that one can obtain the thermopower as a function of temperature and doping level from the band structure without any additional input.

We emphasize that while the CSTA neglects the energy dependence of the scattering rate on energy scales of $k_B T$, as compared to the energy dependence of the electronic structure, it does not involve any assumption about the temperature or doping level dependence of the scattering. Furthermore, the CSTA has been used to successfully describe the Seebeck coefficients and their temperature and doping dependencies in a wide variety of thermoelectric materials. This includes both conventional thermoelectrics^{25,27,29–32}, and even materials where unusual scattering may be expected such as the oxide Na_xCoO_2 ,³³ and PdCoO_2 ,³⁴ which was recently shown to display hydrodynamic electron transport.³⁵ We note that it has been shown to yield results in accord with experiment for SrTiO_3 ,³⁶ which is the subject of the present study. In addition the CSTA has proven useful as a basis for performing high throughput searches for new thermoelectrics.^{37–39} Going beyond the CSTA would require detailed knowledge of the energy dependent scattering mechanisms including different sources of scattering in combination. For example, if one includes only acoustic phonon scattering with τ^{-1} proportional to the density of states, one obtains the result that the mobility diverges and the conductivity is flat as the carrier concentration is lowered to zero. The behavior can be understood from the low T behavior, specifically the density of states is given by $N(\epsilon) = \partial n(\epsilon)/\partial \epsilon$, which for a power law dependence of n on ϵ yields $N(\epsilon) \propto n(\epsilon)/\epsilon$. $\sigma = ne\mu$, where μ is the mobility. For a parabolic band $\epsilon = \hbar^2 k^2/2m$, $n(\epsilon) \propto \epsilon^{3/2}$, $\sigma \propto e^2 \tau n/m$, while density of states $N(\epsilon)$ goes as $\epsilon^{1/2}$, i.e. $n^{1/3}$ so that σ has a sublinear dependence on n , with a divergent mobility, $\mu = \sigma/ne$. At finite T , the flatness of σ/τ is enhanced by the Fermi broadening and the divergence of μ becomes stronger.

This unphysical result comes from ignoring point defect, polar optical phonon and other scattering. It is the case for a parabolic band model and we verified by direct calculation at 300 K that it is also so for the band structure of SrTiO_3 . Defect scattering, will in general limit the mobility and prevent such divergences of the mobility. SrTiO_3 has a large dielectric constant due high Born charges leading to nearness to ferroelectricity. This provides a mechanism for screening of ionized impurity and other defect scattering.⁴⁰ In SrTiO_3 the dielectric constant and therefore this source of screening is a strong function of temperature. The polar nature of the compound and the high Born charges lead to the expectation of strong polar optical phonon scattering. Himmetoglu and co-workers find that at room temperature with moderate carrier concentration this scattering mechanism dominates the mobility and that it has a strong and complex momentum dependence,⁴¹ and a complex energy dependence may also be expected in analogy with other materials.⁴² Furthermore, one expects acoustic phonon scattering, discussed above, to contribute to scattering in any material, and electron-electron scattering may also contribute for heavy doping and low temperature.

It is possible to fit various energy, doping and temperature dependent scattering terms to experiment for semiconductors for which large amounts of doping and temperature dependent data is available. An example is provided by the detailed fits performed for the Pb chalcogenide IV-VI semiconductor thermoelectrics, which reproduced extremely well the known body of experimental data.^{43–45} These models may, however, have limited predictive ability outside the range of known data due to the large number of fitting parameters used. For example, they lead to the expectation that the ZT for PbTe could not exceed unity and that PbSe would invariably be inferior to PbTe. In contrast, calculations based on the CSTA, similar to the approach followed here, did predict that ordinarily (Na and/or K) but heavily doped p-type PbTe and PbSe would both have high ZT above unity,^{25,46} as was subsequently shown to be the case.⁴⁷ Therefore we use the CSTA, which while approximate, allows one to predict the thermopower directly from the first principles electronic structure, with no adjustable parameters.

In the present work, we use results calculated from the electronic structure using the CSTA and combine these models derived by fitting experimental data for the temperature and doping concentration dependent relaxation time τ and lattice thermal conductivity, κ_L , to obtain the conductivity and thermal conductivity. Eventually we are able to get the figure of merit ZT in terms of T and n .

The band structure calculations were performed with the linearized augmented plane wave (LAPW) method⁴⁸, as implemented in the WIEN2K code⁴⁹. We used LAPW sphere radii of 2.5 bohr for Sr, 1.9 bohr for Ti and 1.75 bohr for O. A k-point mesh of $6 \times 6 \times 6$ was used for total energy calculations and much denser k meshes are used for density of states ($17 \times 17 \times 17$), isoenergy surfaces and transport properties ($27 \times 27 \times 27$). We adopted the experimental cubic structure with lattice constant $a = 3.906 \text{ \AA}$ ⁵⁰, with the modified Becke-Johnson (mBJ) potential of Tran and Blaha⁵¹. This potential generally gives improved band gaps for simple semiconductors and insulators^{25,51,52}. Spin-orbit coupling (SOC) was included in all the calculations.

III. RESULTS AND DISCUSSION

SrTiO_3 is a band insulator with a band gap value of 3.2 eV.⁵³ Our calculated band structure agrees with this quite well as shown in Fig. 1. The calculated band gap is about 2.68 eV (R- Γ) with SOC using mBJ potential. At the Γ point near the conduction band minimum (CBM), the lowest three bands are largely from Ti $3d$ - t_{2g} states and the degeneracy is lifted by SOC effects with a split-off energy of about 30 meV. This agrees reasonably with other theoretical calculations (25-28 meV^{54,55}) and experiment (17 meV⁵⁶) by interband Raman scattering. The electronic

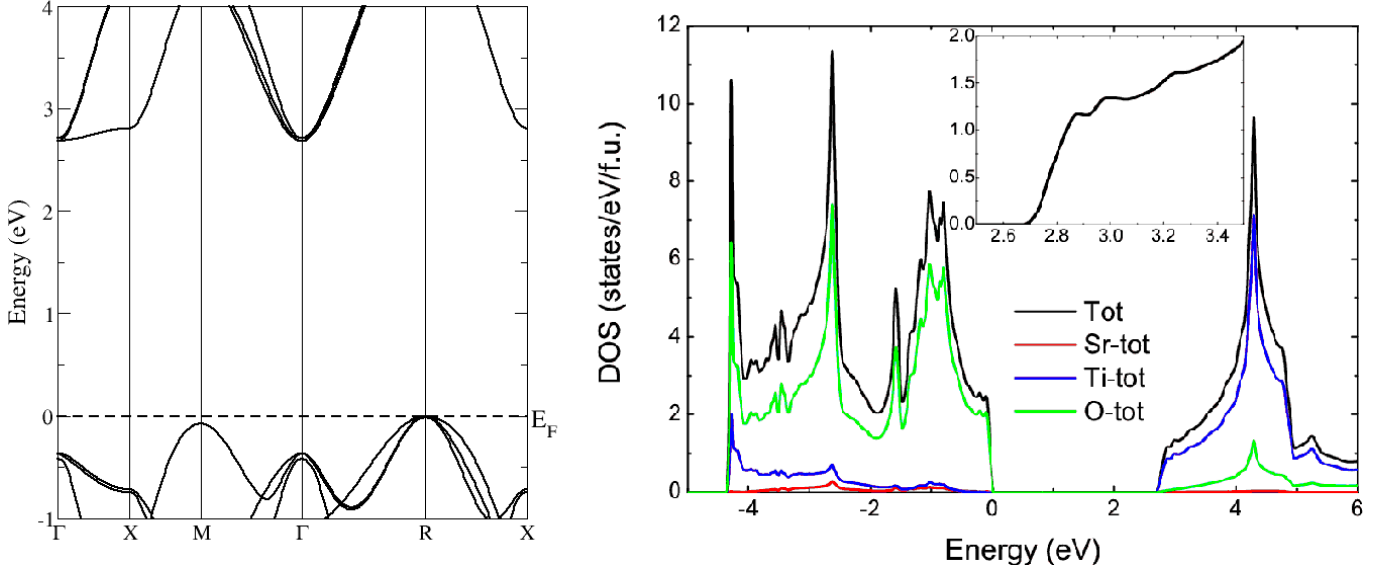


FIG. 1: Calculated band structure and total density of states of SrTiO₃ with mBJ and spin-orbit coupling. The inset shows the detailed feature near CBM. Density of states are shown per SrTiO₃ formula unit (f.u.). Energy zero is set at the valence band maximum.

density of states (DOS) is presented in the right panel of Fig. 1, where the inset shows the details at the CBM. As known, the valence band is mainly derived from oxygen $2p$ states and the conduction band is dominated by Ti $3d$ states especially near CBM. In fact the high S in STO is mainly due to the large DOS effective mass^{57,58}.

Within a simple parabolic band model, the $S(T)$ is proportional to effective mass (m^*) and decreases as the $2/3$ power of doping concentration. Moreover, m^* plays different roles in σ and S . For thermoelectric performance it is important to have both high S and high σ , which as discussed previously⁵⁹ have opposite dependences on both carrier concentration and effective mass. This conundrum can be resolved by certain complex band structures that exploit the different transport integrals that enter σ and S ^{60–66}. STO has a particular band shape arising from the degeneracy of the t_{2g} levels in an octahedral crystal field that gives effectively lower dimensional behaviour in transport even though the material is cubic, analogous to the case of PbTe⁶⁵. The sharp onset of the DOS at the CBM reflects the low-dimensional nature of the electronic structure.

The temperature and doping concentration dependent Seebeck coefficient, $S(T, n)$, can be obtained directly from the electronic structure with no adjustable parameters within CSTA. From the Wiedemann-Franz relation one can rewrite ZT as $ZT = rS^2/L$ where $r = \kappa_e/(\kappa_e + \kappa_l)$ and $L = 2.45 \times 10^{-8} \text{ W}\Omega/\text{K}^2$ is the standard Lorenz number. If κ_l is neglected assuming the upper bound of ZT which can reach unity when $S = 156 \mu\text{V}/\text{K}$. In reality good TE materials usually have S larger than $200 \mu\text{V}/\text{K}$. We illustrate the calculated $S(T, n)$ of n -type STO at different temperatures in Fig. 2 (a). As seen, high Seebeck coefficients ($> 200 \mu\text{V}/\text{K}$) are obtained even at quite low temperatures (200 K) with doping concentration up to 10^{20} cm^{-3} . At high temperatures ($> 1000 \text{ K}$), S exceeds $200 \mu\text{V}/\text{K}$ at high doping concentrations ($\sim 10^{21} \text{ cm}^{-3}$). Importantly, due to the substantial band gap, there is no bipolar effect and therefore S keeps increasing with T to high temperatures even at low doping concentrations.

Within the framework of CSTA, one can obtain σ/τ directly from the electronic structure as a function of n and T . However, it is not possible to get σ without the knowledge of the scattering rate τ^{-1} . Therefore, in order to proceed, we used the strategy of our recent work on $\text{Mg}_2(\text{Ge}, \text{Sn})$ ⁶⁷ and a prior model on PbSe where the experimental data was used to fit the relaxation time τ . For this purpose, the extrapolation of the experimental data was based on the recent work of La-doped STO films grown by hybrid molecular beam epitaxy, conducted by Cain and co-workers⁶⁸. Their samples have relatively higher electrical conductivities at the same conditions (T and n) compared to other studies, which may indicate the higher quality of the STO films. Specifically, we used the data set which has the highest σ and choose the experimental S at corresponding T with a value of about $-270 \mu\text{V}/\text{K}$ at 300 K. The reason is that we want to estimate the optimum ZT , and the choice of the best samples as the baseline minimizes the effects on the predicted ZT due to extrinsic effects that are presumably controllable. By comparing with our calculated $S(T, n)$ (Fig. 2 (a)), we obtain the carrier concentration $n = 8.4 \times 10^{19} \text{ cm}^{-3}$. This calculated n is smaller than the reported one ($2 \times 10^{20} \text{ cm}^{-3}$). We are using the experimental S rather than the nominal carrier concentration because of the potential neglect of compensating defects as well as the fact that the carrier concentration is not the same as in the Hall measurements for a non-parabolic case. At this temperature and doping concentration, combining with the calculated

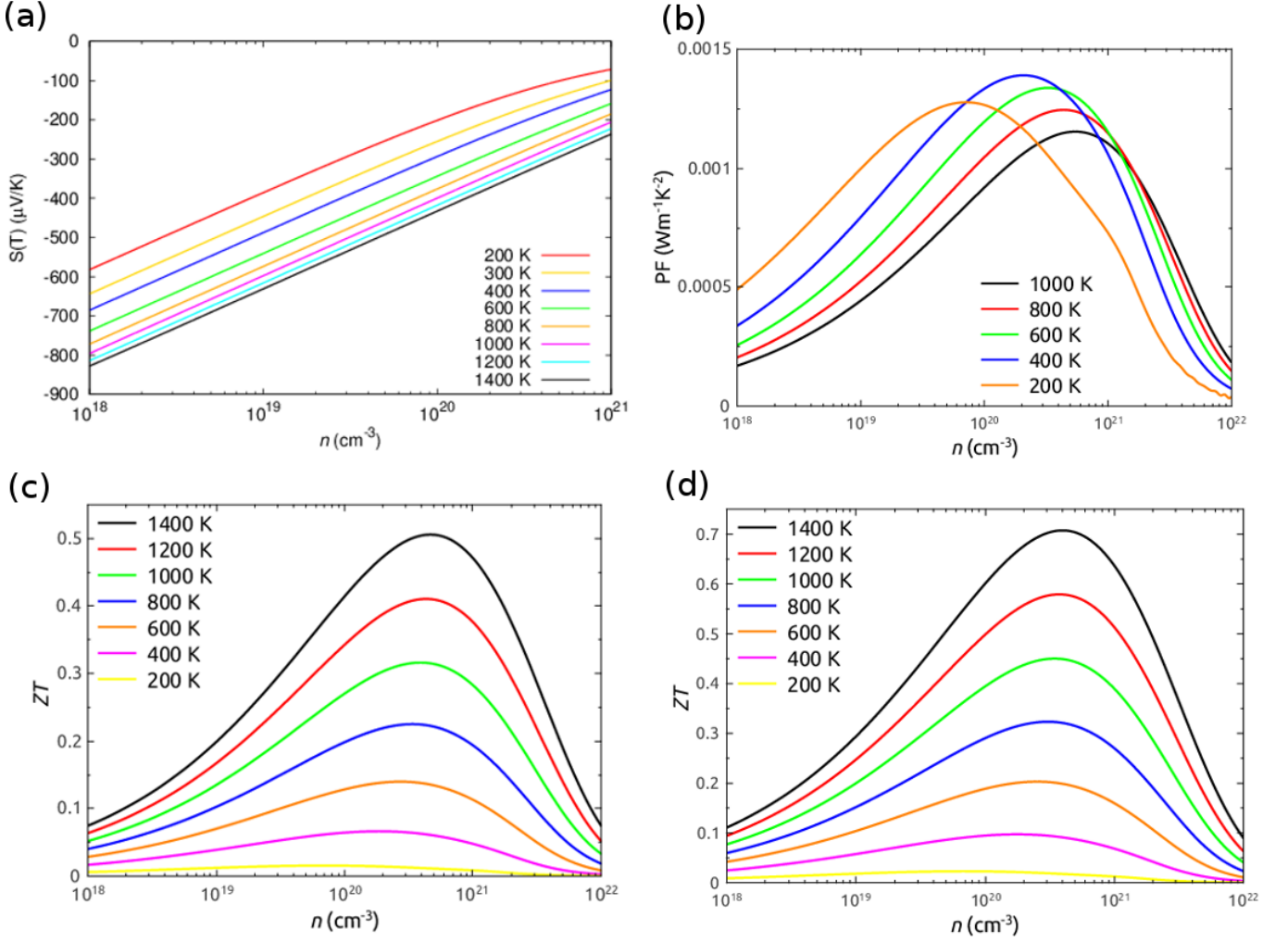


FIG. 2: Calculated thermoelectric properties for n -type STO: (a) $S(T, n)$, (b) power factor, (c) ZT using the bulk κ at 300 K and (d) ZT using smaller κ (see text).

σ/τ and experimental σ ($\sim 18500 \text{ } \Omega^{-1}\text{m}^{-1}$)⁶⁸ yields $\tau = 7.2 \times 10^{-15} \text{ s}$. In this regime, we considered an approximate electron-phonon T dependence of τ where τ is proportional to T^{-1} and decreases with carrier concentration as $n^{-1/3}$. Therefore these together with fitted τ yield $\tau = 9.45 \times 10^{-6} T^{-1} n^{-1/3}$ with τ in s, T in K and n in cm^{-3} . Thus σ can be calculated through $\sigma/\tau \times \tau$. The corresponding PF (σS^2) obtained from the calculated $S(T, n)$ and σ as mentioned above is presented in Fig. 2 (b). The maximum PF is about $1.4 \times 10^{-3} \text{ Wm}^{-1}\text{K}^{-2}$ at 400 K, which is smaller than the heavily La doped STO ($3.6 \times 10^{-3} \text{ Wm}^{-1}\text{K}^{-2}$) at room temperature¹⁹. Moreover, the position of the peak in the PF as a function of carrier concentration shifts to higher doping levels with increasing T . This means that optimization of the carrier concentration for high temperature will lead to higher doping levels than are optimum at lower T . Thermal conductivity is also required to assess ZT . As mentioned, κ is composed of both the lattice and electronic contributions. The electronic part can be directly calculated using the Wiedemann-Franz relation from $\kappa_e = L\sigma T$. The lattice thermal conductivity usually behaves as T^{-1} until high temperatures, as also observed in the experiments²¹. Hence we estimate κ as $\kappa = A/T + L\sigma T$ with constant A determined by fitting the experimental data of κ_l . There have been a number of studies of the thermal conductivity measurements on both the bulk and doped STO at elevated temperatures^{20–24,69–72}. Due to the significant difference of κ between bulk and heavily doped materials, we consider two scenarios with one taking the bulk κ at 300 K ($\sim 11 \text{ Wm}^{-1}\text{K}^{-1}$)^{21,71} and the other using the doped κ at the same T ($\sim 8 \text{ Wm}^{-1}\text{K}^{-1}$, based on moderately doped samples^{21,24}). With the second scenario, we are able to get low κ from 2.3 - 2.5 $\text{Wm}^{-1}\text{K}^{-1}$ at 1000 K. These values are in better accord with experiments at high temperatures ($\sim 1000 \text{ K}$).

Finally, we obtain the ZT as a function of temperature and doping concentration. The results are shown in Figs. 2 (c) and (d) with (c) depicting the data from model with bulk κ . Although it has a number of assumptions, the

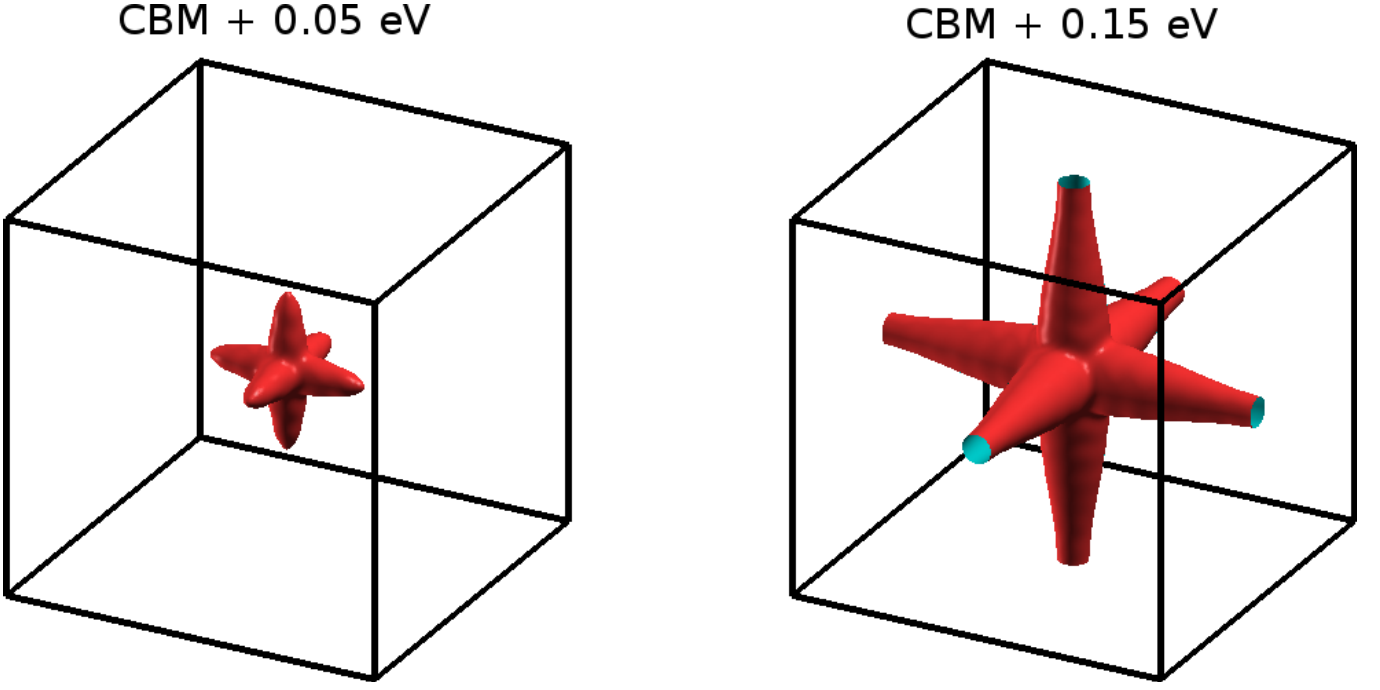


FIG. 3: Isoenergy surfaces at 0.05 eV and 0.15 eV above CBM for n -type STO. Note the low-dimensional-like intersecting cylinders in higher carrier concentration (right panel) that originated from the t_{2g} orbitals is beneficial for achieving high ZT .

model can be used to describe the behaviour of ZT with respect to T and n . As seen, ZT strongly depends on T and increases up to the highest T . This is mainly due to the substantial band gap so that the Seebeck coefficient keeps increasing to high T . The lattice thermal conductivity decreases at high T but the electronic part has weaker T dependence. The maximum ZT with bulk κ (Fig. 2 (c)) is about 0.5 at 1400 K and 0.3 at 1000 K with high doping concentration range ($\sim 4\text{-}5 \times 10^{20} \text{ cm}^{-3}$). By using smaller κ , about 40% higher ZT can be obtained, as shown in Fig. 2 (d), with a peak ZT value up to 0.7 at 1400 K and 0.45 at 1000 K with similar doping level ($\sim 3\text{-}4 \times 10^{20} \text{ cm}^{-3}$). Though a little higher in the latter case, our calculated ZT with both experimental range κ agree reasonably well with existing experiments ($\sim 0.2\text{-}0.4$ at 900 K - 1000 K^{21-24,70}). Complex isoenergy surfaces are favorable for electronic performance as mentioned above. Therefore we studied the isoenergy surfaces of cubic STO especially at the peak ZT values, for instance at 1400 K and 600 K with doping concentration of $5 \times 10^{20} \text{ cm}^{-3}$ and $3 \times 10^{20} \text{ cm}^{-3}$ as shown in Fig. 2 (c). However we found the Fermi energy is about 0.12 eV (for 1400 K) below and 0.002 eV (600 K) above CBM at corresponding carrier concentrations due to the heavy onset feature at the CBM. Thus we present the isoenergy surfaces at 0.05 eV and 0.15 eV above CBM. As seen in Fig. 3, the surfaces show complex shapes due to the three lowest t_{2g} orbitals. Specifically, the surfaces in the 0.15 eV case consist of intersecting cylinders joined at the center around Γ and two small sections inside the center, as was discussed previously for STO and other d^0 cubic perovskites⁵⁹. This low-dimensional-like intersecting cylinders in higher carrier concentration (right panel of Fig. 3) that originated from the t_{2g} orbitals is beneficial for achieving high ZT . Thus high doping concentration will be advantageous in achieving high thermoelectric performance for cubic STO.

IV. SUMMARY AND CONCLUSIONS

In summary, we have investigated the electronic and thermoelectric properties of SrTiO_3 . Using the combination of constant scattering time approximation Boltzmann theory based on first-principles electronic structure and existing experiments, we have predicted the thermoelectric performance of STO, including the Figure of merit, ZT . Importantly, we find high ZT value of 0.7 at high temperature (1400 K). This confirms the potential of high temperature thermoelectric properties of STO. We find ZT can be further improved relative to currently reported experimental values via carrier concentration optimization.

Acknowledgments

We are grateful for helpful discussions with Susanne Stemmer. This work was supported by the Department of Energy through the S3TEC Energy Frontier Research Center award # DE-SC0001299/DE-FG02-09ER46577.

-
- * Electronic address: singhdj@missouri.edu
- ¹ C. Wood, Rep. Prog. Phys. **51**, 459 (1988).
 - ² J. Yang and T. Caillat, MRS Bull. **31**, 224 (2006).
 - ³ G. J. Snyder and E. S. Toberer, Nat. Mater. **7**, 105 (2008).
 - ⁴ I. Matsubara, R. Funahashi, T. Takeuchi, S. Sodeoka, T. Shimizu, and K. Ueno, Appl. Phys. Lett. **78**, 3627 (2001).
 - ⁵ T. Tsubota, M. Ohtaki, K. Eguchi, and H. Arai, J. Mater. Chem. **7**, 85 (1997).
 - ⁶ J. He, Y. Liu, and R. Funahashi, J. Mater. Res. **26**, 1762 (2011).
 - ⁷ G. Saucke, S. Populoh, P. Thiel, W. J. Xie, R. Funahashi, and A. Weidenkaff, J. Appl. Phys. **118**, 035106 (2015).
 - ⁸ O. Yamashita, S. Tomiyoshi, and K. Makita, J. Appl. Phys. **93**, 368 (2003).
 - ⁹ X. Shi, J. Yang, J. R. Salvador, M. Chi, J. Y. Cho, H. Wang, S. Bai, J. Yang, W. Zhang, and L. Chen, J. Am. Chem. Soc. **133**, 7837 (2011).
 - ¹⁰ G. S. Nolas, M. Kaeser, R. T. Littleton, and T. M. Tritt, Appl. Phys. Lett. **77**, 1855 (2000).
 - ¹¹ I. Terasaki, Y. Sasago, and K. Uchinokura, Phys. Rev. B **56**, R12685 (1997).
 - ¹² K. Koumoto, I. Terasaki, and R. Funahashi, MRS Bulletin **31**, 206 (2006).
 - ¹³ K. Fujita, T. Mochida, and K. Nakamura, in *Thermoelectrics, 2001. Proceedings ICT 2001. XX International Conference on* (2001), pp. 168–171.
 - ¹⁴ M. Shikano and R. Funahashi, Appl. Phys. Lett. **82**, 1851 (2003).
 - ¹⁵ K. P. Ong, D. J. Singh, and P. Wu, Phys. Rev. B **83**, 115110 (2011).
 - ¹⁶ M. Ohtaki, K. Araki, and K. Yamamoto, J. Electron. Mater. **38**, 1234 (2009).
 - ¹⁷ P. Jood, R. J. Mehta, Y. Zhang, G. Peleckis, X. Wang, R. W. Siegel, T. Borca-Tasciuc, S. X. Dou, and G. Ramanath, Nano Lett. **11**, 4337 (2011).
 - ¹⁸ P. Jood, R. J. Mehta, Y. Zhang, T. Borca-Tasciuc, S. X. Dou, D. J. Singh, and G. Ramanath, RSC Adv. **4**, 6363 (2014).
 - ¹⁹ T. Okuda, K. Nakanishi, S. Miyasaka, and Y. Tokura, Phys. Rev. B **63**, 113104 (2001).
 - ²⁰ H. Muta, K. Kurosaki, and S. Yamanaka, J. Alloys Compd **392**, 306 (2005).
 - ²¹ S. Ohta, T. Nomura, H. Ohta, and K. Koumoto, J. Appl. Phys. **97**, 034106 (2005).
 - ²² H. C. Wang, C. L. Wang, W. B. Su, J. Liu, Y. Sun, H. Peng, and L. M. Mei, J. Am. Ceram. Soc. **94**, 838 (2011).
 - ²³ S. R. Popuri, A. J. M. Scott, R. A. Downie, M. A. Hall, E. Suard, R. Decourt, M. Pollet, and J.-W. G. Bos, RSC Adv. **4**, 33720 (2014).
 - ²⁴ Z. Lu, H. Zhang, W. Lei, D. C. Sinclair, and I. M. Reaney, Chem. Mater. **28**, 925 (2016).
 - ²⁵ D. Parker and D. J. Singh, Phys. Rev. B **82**, 035204 (2010).
 - ²⁶ J. M. Ziman, *Principles of the Theory of Solids, 2nd Edition* (Cambridge University Press, Cambridge, 1972).
 - ²⁷ G. Madsen and D. J. Singh, Computer Phys. Commun. **175**, 67 (2006).
 - ²⁸ L. Zhang and D. J. Singh, Phys. Rev. B **80**, 075117 (2009).
 - ²⁹ J. Yang, H. M. Li, T. Wu, W. Q. Zhang, L. D. Chen, and J. H. Yang, Adv. Funct. Mater. **18**, 2880 (2008).
 - ³⁰ D. Parker and D. J. Singh, Phys. Rev. X **1**, 021005 (2011).
 - ³¹ R. Fei, A. Faghaninia, R. Soklaski, J. A. Yan, C. Lo, and L. Yang, Nano Lett. **14**, 6393 (2014).
 - ³² L. Bjerg, G. K. H. Madsen, and B. B. Iversen, Chem. Mater. **23**, 3907 (2011).
 - ³³ D. J. Singh and D. Kasinathan, J. Electron. Mater. **36**, 736 (2007).
 - ³⁴ K. P. Ong, D. J. Singh, and P. Wu, Phys. Rev. Lett. **104**, 176601 (2010).
 - ³⁵ P. J. W. Moll, P. Kushwaha, N. Nandi, B. Schmidt, and A. P. Mackenzie, Science **351**, 1061 (2016).
 - ³⁶ A. Kinaci, C. Cevik, and T. Cagin, Phys. Rev. B **82**, 155114 (2010).
 - ³⁷ G. K. H. Madsen, J. Am. Chem. Soc. **128**, 12140 (2006).
 - ³⁸ S. Wang, Z. Wang, W. Setyawan, N. Mingo, and S. Curtarolo, Phys. Rev. X **1**, 021012 (2011).
 - ³⁹ S. Curtarolo, G. L. W. Hart, M. B. Nardelli, N. Mingo, S. Sanvito, and O. Levy, Nature Materials **12**, 191 (2013).
 - ⁴⁰ M. H. Du and D. J. Singh, Phys. Rev. B **81**, 144114 (2010).
 - ⁴¹ B. Himmetoglu, A. Janotti, H. Peelaers, A. Alkauskas, and C. G. Van de Walle, Phys. Rev. B **90**, 241204 (2014).
 - ⁴² S. M. Komirenko, K. W. Kim, M. A. Strosio, and M. Dutta, Phys. Rev. B **61**, 2034 (2000).
 - ⁴³ Y. I. Ravich, B. A. Efimova, and V. I. Tamarchenko, Phys. Status Solidi B **43**, 11 (1971).
 - ⁴⁴ Y. I. Ravich, B. A. Efimova, and V. I. Tamarchenko, Phys. Status Solidi B **43**, 453 (1971).
 - ⁴⁵ Y. I. Ravich, *Semiconducting Lead Chalcogenides* (Springer, Berlin, 1970).
 - ⁴⁶ D. J. Singh, Phys. Rev. B **81**, 195217 (2010).
 - ⁴⁷ Y. Pei, A. LaLonde, S. Iwanaga, and G. J. Snyder, Energy Environ. Sci. **4**, 2085 (2011).
 - ⁴⁸ D. J. Singh and L. Nordstrom, *Planewaves, Pseudopotentials and the LAPW Method, 2nd Edition* (Springer, Berlin, 2006).
 - ⁴⁹ K. Schwarz, P. Blaha, and G. Madsen, Computer Phys. Commun. **147**, 71 (2002).
 - ⁵⁰ L. Cao, E. Sozontov, and J. Zegenhagen, physica status solidi (a) **181**, 387 (2000).

- ⁵¹ F. Tran and P. Blaha, Phys. Rev. Lett. **102** (2009).
- ⁵² D. J. Singh, Phys. Rev. B **82**, 205102 (2010).
- ⁵³ M. Cardona, Phys. Rev. **140**, 651 (1965).
- ⁵⁴ L. F. Mattheiss, Phys. Rev. B **6**, 4718 (1972).
- ⁵⁵ J. D. Baniecki, M. Ishii, H. Aso, K. Kurihara, and D. Ricinschi, J. Appl. Phys. **113**, 013701 (2013).
- ⁵⁶ H. Uwe, T. Sakudo, and H. Yamaguchi, Jpn. J. Appl. Phys. **24**, 519 (1985).
- ⁵⁷ H. P. R. Frederikse, W. R. Thurber, and W. R. Hosler, Phys. Rev. **134**, A442 (1964).
- ⁵⁸ H. Ohta, K. Sugiura, and K. Koumoto, Inorg. Chem. **47**, 8429 (2008).
- ⁵⁹ G. Xing, J. Sun, K. P. Ong, X. Fan, W. Zheng, and D. J. Singh, APL Mater. **4**, 053201 (2016).
- ⁶⁰ K. Kuroki and R. Arita, J. Phys. Soc. Jpn **76**, 083707 (2007).
- ⁶¹ X. Chen, D. Parker, and D. J. Singh, Sci. Rep. **3**, 3168 (2013).
- ⁶² H. Usui, K. Suzuki, K. Kuroki, S. Nakano, K. Kudo, and M. Nohara, Phys. Rev. B **88**, 075140 (2013).
- ⁶³ H. Usui, S. Shibata, and K. Kuroki, Phys. Rev. B **81**, 205121 (2010).
- ⁶⁴ K. Shirai and K. Yamanaka, J. Appl. Phys. **113**, 053705 (2013).
- ⁶⁵ D. Parker, X. Chen, and D. J. Singh, Phys. Rev. Lett. **110**, 146601 (2013).
- ⁶⁶ N. A. Mecholsky, L. Resca, I. L. Pegg, and M. Fornari, Phys. Rev. B **89**, 155131 (2014).
- ⁶⁷ J. Sun and D. J. Singh, Phys. Rev. Applied **5**, 024006 (2016).
- ⁶⁸ T. A. Cain, A. P. Kajdos, and S. Stemmer, Appl. Phys. Lett. **102**, 182101 (2013).
- ⁶⁹ C. Yu, M. L. Scullin, M. Huijben, R. Ramesh, and A. Majumdar, Appl. Phys. Lett. **92**, 191911 (2008).
- ⁷⁰ N. Wang, H. Chen, H. He, W. Norimatsu, M. Kusunoki, and K. Koumoto, Sci. Rep. **3**, 3449 (2013).
- ⁷¹ D.-W. Oh, J. Ravichandran, C.-W. Liang, W. Siemons, B. Jalan, C. M. Brooks, M. Huijben, D. G. Schlom, S. Stemmer, L. W. Martin, et al., Appl. Phys. Lett. **98**, 221904 (2011).
- ⁷² H. Muta, K. Kurosaki, and S. Yamanaka, J. Alloys Compd. **350**, 292 (2003).